Article

The Simulation Study on Indoor Heat and Moisture Transfer Characteristics of an Ancient Palace Building in Beijing

Fang Liu, Xiaofen Zhang, Jiarui Zeng, Yafei Li and Gang Wang*

School of Environmental and Energy Engineering, Beijing University of Civil Engineering and Architecture, Beijing, China

* Correspondence: wanggang@bucea.edu.cn

Abstract: The heritage of ancient buildings is an important part of the world's history and culture, which has an extremely rich historical-cultural value and artistic research value. Beijing has a large number of palace ancient buildings, and because of the age of their construction, many of them have problems of varying degrees of peeling and mold on the inner surfaces of the envelope. To solve the problems of the damp and moldy interior of palace buildings, a mathematical model of indoor heat and moisture transfer was established based on a wooden palace ancient building in Beijing. Through the indoor mold distribution validation model, the effects of outdoor humidity, soil moisture, wall humidity, and other factors on the indoor heat and moisture transfer of ancient buildings were simulated and analyzed by using the control variables method. The results showed that the molds were distributed at the indoor corners and floors, and the simulation of indoor humidity match the measured humidity. Thus, the simulation results were consistent with the actual situation. The variable trend of the relative humidity of the indoor environment with the outdoor humidity is inconsistent from plane to plane, i.e. it increases or remains constant with the increase of the outdoor humidity. The indoor ambient relative humidity increased with increasing the wall humidity. And the indoor average temperature is 23.3 ℃ and indoor relative humidity ranged between 90.9 % to 92.44 %. Soil moisture and wall humidity were the main factors affecting the indoor environmental relative humidity.

Keywords: ancient building; heat transfer moisture transfer; simulation

1. Introduction

Ancient buildings are an important part of the world's historical and cultural heritage, which are an important carrier for inheriting national traditional culture and promoting cultural exchanges among nations and cannot be restored once they are damaged [1]. Nowadays, the protection of cultural relics and ancient buildings is getting more and more attention. "Preserve the original appearance" is the basic principle for the protection of ancient buildings, so higher requirements for the technology of protection and restoration of ancient buildings have been proposed. With the advancement of technology, the conservation and repair of ancient buildings have gradually incorporated modern simulation and digital means from a purely manual approach [2,3] to seek the root mechanism of problem-solving.

To better preserve its original appearance and historical value, revitalize the social value of ancient buildings, and enhance the comfort of visitors, many researchers have been conducting various explorations in recent years [4-7]. For example, ancient building wall repair work and ancient architecture of digital protection, etc. The typical problems of ancient building damage are the degradation of the anti-corrosion paint surface and the moldy wood structure. It was found that the deterioration and mold problems of ancient buildings are influenced by the coupling of multiple

 doi:10.20944/preprints202305.1338.v1

factors such as the thermal and humid environment around the building, air flow, underground soil moisture, and the building envelope, etc [8-10]. Exploring the patterns of influence of different factors on the deterioration of ancient buildings is an important prerequisite for taking effective conservation measures. At present, numerical simulation methods investigating the effects of airflow, envelope structure, soil, precipitation and other factors on the heat and moisture migration of ancient buildings is a low-cost and high-efficiency way to grasp the influence law and degree of ancient building damage and can put forward effective protection schemes for the problems such as damp and mold. Therefore, it is especially important to carry out more in-depth research and analysis based on numerical simulation methods for ancient buildings and propose reasonable conservation plans. Hong et al. [11] used the software CFD to study the indoor wet environment and linearly fitted the factors affecting humidity, and concluded that the predicted humidity distribution was in good agreement with the experiment. Liu [12] focused on and studied the insulation technology of ancient buildings in the Amu River basin, using AIRPAK software to simulate and analyze the indoor temperature of ancient buildings and explore the effect of active heating measures, the results showed that with a cross-section of the building height average temperature rise gradually, residential buildings adaptation to cold climate gradually enhanced. Teodosiu et al. [13] investigated numerical models for assessing thermal comfort, and developed CFD numerical models for airflow modeling and humidity modeling of indoor air, then analyzed and demonstrated the good potential for correctly estimating the indoor environment under stable and uniform thermal conditions. Bi et al. [14] conducted an experimental and numerical analysis of the moisture and heat transfer in the cave walls of the Mogao Caves using a comparison of simulation results with experimental temperature and relative humidity values, finding that temperature changes may lead to condensation of moisture in the air, and the application of the one-dimensional model to simulate the cave wall has limitations. Balocco et al. [15] adopted CFD software to carry out a three-dimensional transient simulation of the natural ventilation system of a historical building library in Italy and explored the operation mode of the natural ventilation system inside the building, which confirmed that the ancient building could create a good natural ventilation environment. Li et al. [16] analyzed the hygrothermal environment of the Luohan Hall of Baosheng Temple located in the southeast of China and concluded that the air temperature near the sculpture had different fluctuation modes under different directions, and the relative air humidity fluctuated violently. Cao et al. [17] used the CFD software Fluent to numerically simulate the air movement, temperature, and relative humidity of the micro-environment in the museum, and concluded that the large gradient of temperature and humidity distribution was not conducive to the preservation of artifacts. In addition, some scholars have studied numerical simulation for the cultural heritage of wooden structures. Huijbregts et al. [18] conducted a two-dimensional multi-area building simulation on a wooden cabinet in a Dutch castle to study the influence of indoor climate changes on the heat and humidity of the cabinet and concluded that indoor climate conditions were controlled by humidity rather than restricted by the average water content of the room. Napp et al. [19] studied the different indoor climate control schemes of a church in Estonia through field measurement and simulation and concluded that dehumidification measures could be used to prevent mold growth and protect wood parts from cracking. Apart from the relevant research on heat and humidity transfer in residential buildings, existing literature has also investigated building types such as libraries, temples, churches, and grottoes.

The object of this study is the world's most complete surviving palace-type ancient building with a construction history of 600 years. The three-dimensional heat and moisture transfer characteristics of palace-style wooden ancient buildings in Beijing are studied. A mathematical model of indoor heat and moisture transfer is established, and the model is verified by indoor mold growth and comparison with actual measured data. The influences of outdoor humidity environment, soil moisture, wall humidity, and other factors on the indoor heat and moisture transfer characteristics of ancient buildings are analyzed, and the main protection measures of ancient buildings are proposed. The research results provide effective theoretical guidance for the conservation of palace-style wooden ancient buildings in Beijing.

Preprints (www.preprints.org) | NOT PEER-REVIEWED | Posted: 18 May 2023 doi:10.20944/preprints202305.1338.v1

2. Indoor and outdoor heat and humidity environment testing of ancient buildings

2.1. Overview of ancient buildings

The palace-style buildings in Beijing are one of the largest and best-preserved wooden ancient buildings in the world, which have a variety of architectural structures with more than 70 different building types [20]. In this study, a palace-style wooden ancient building in Beijing is selected as the research object. The building is located on the west side of the palace-style building complex in Beijing, which was built during the Jiajing period of the Ming Dynasty.

2.2. Outdoor environmental parameters

According to the data statistics of a weather station in Beijing (https://www.xihe-energy.com/), the outdoor temperature and humidity change curve of the ancient building is shown in Figure 1. Through the investigation and analysis of the environmental monitoring of ancient buildings, the relative humidity of the indoor environment of the ancient building is high in summer. The original appearance of the building is damaged by the humid indoor environment. Therefore, the outdoor ambient temperature and humidity in July 2022 are selected and the average value is taken as the selection of outdoor meteorological parameters. The outdoor environmental temperature is 26.3 ℃, relative humidity is 67.17 %, and atmospheric pressure is 101.35 kPa. The moisture content is 14.49 g/kg $_{dry\ air}$, water vapor partial pressure is 2.3073 kPa.

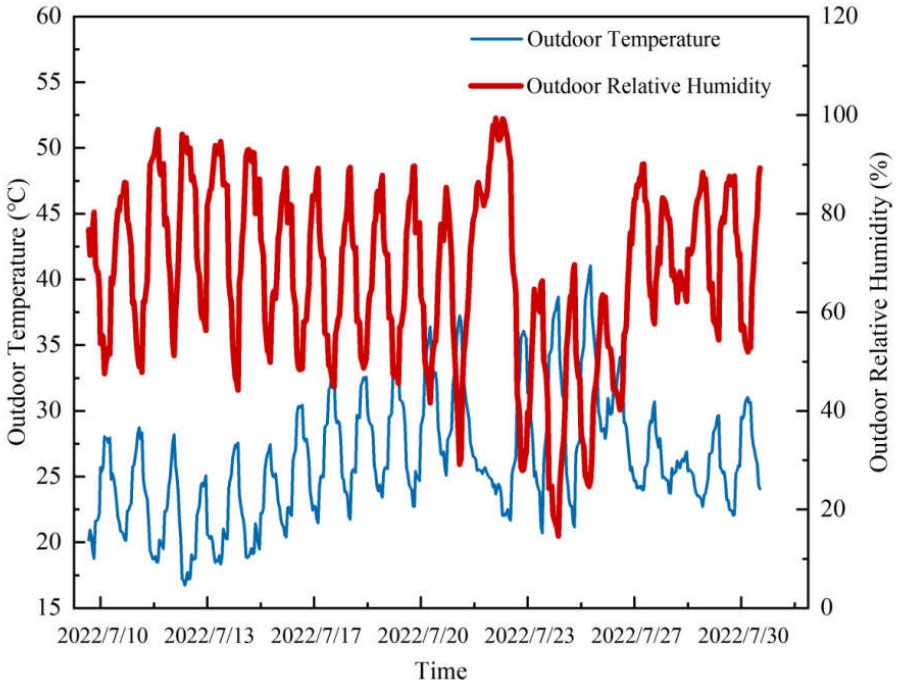

Figure 1. Outdoor temperature and humidity change curve.

2.3. Indoor environmental parameters

Based on the relevant research [21], the indoor air temperature is 24.7 ℃, the indoor relative humidity is 75 %, the moisture content is 14.67 g/kg $_{dry\ air}$, and the water vapor partial pressure is 2.3347 kPa. The indoor relative humidity of the interior walls is 92 %, the moisture content is 18.09 g/kg $_{dry\ air}$, and the water vapor partial pressure is 2.8639 kPa.

2.4. Indoor flooring parameters

Soil temperature and humidity can have an impact on the coupled heat and moisture transfer [22]. The ground temperature is set at 23.3 °C, and the water absorption rate of ancient grey bricks

Preprints (www.preprints.org) | NOT PEER-REVIEWED | Posted: 18 May 2023 doi:10.20944/preprints202305.1338.v1

generally ranges from 14 % to 25 % [23], so the water absorption rate of grey bricks is set at 14 % in this work. Beijing located in the North China Plain is sandy soil. According to relevant studies [21,24], the soil volumetric moisture content of ancient buildings in the area is 0.09 m^3/m^3. The field capacity of sandy soils in the North China Plain is 10 % -- 14 %. The soil bulk density value of this study is selected from the Second National Soil Survey in China (SNSSC), and the reference value is 0.95 g/cm^3. The conversion relationship between soil relative humidity and soil volumetric water content is [25]:

$$\theta_V = R \times f_C \times S_C \quad (1)$$

where: θ_V is soil volumetric water content, m^3/m^3. R is soil relative humidity, %. f_C is soil field capacity (taken as 10 %). S_C is soil bulk density, kg/m^3.

Consequently, it is calculated that the relative soil humidity of the indoor building ground is 81.5 %, the moisture content is 15.97 g/kg $_{dry\ air}$, and the water vapor partial pressure is 2.5371 kPa.

3. Numerical simulation

3.1. Physical Model

The physical graphic of the ancient building is shown in Figure 2. The main area of the ancient building is 26.63 m^2 and the height of a hard roof is 2.73 m. Its building envelope structure mainly includes a roof, walls, doors and windows, indoor floor, composed of a variety of building structures and components of different materials. The specific structure and its adjustment effect on the environment are shown in Table 1. Table 2 shows the dimensions of the ancient building envelope. After simplifying the physical graphic, the sample point location and building structure of the physical model is shown in Figure 3.

Preprints (www.preprints.org) | NOT PEER-REVIEWED | Posted: 18 May 2023 doi:10.20944/preprints202305.1338.v1

Table 1. Composition and Role of the ancient architecture building envelope

Building envelope types	Structural composition	Regulation of the environment
Roof	Tiles, tile mud, bottom tile, clip ridge ash, gray back, watch board, etc.	It can buffer the external temperature, heat insulation, heat preservation, windproof, rainproof, and so on.
Interior wall	Papering, gold cladding earthen wall, oil-painting ground layer, etc.	It has the functions of being windproof, waterproof, and blocking solar radiation.
Exterior wall	Wall brick masonry, plaster layer, bonding material	It can buffer the change of external temperature, has thermal insulation performance, and blocks indoor and outdoor air circulation.
Doors and windows	Embrace frame, Geshan door, glass, threshold, metal components, finish coat layer, internal papering	The doors and windows composed of wood and glass can reduce indoor and outdoor ventilation and buffer temperature changes to a certain extent.
Interior flooring	There is a kang under the indoor brick of the building.	The indoor ground plays an important role in isolating underground moisture; the indoor ground of the kang system has the effect of heat conduction.
Roof	Tiles, tile mud, bottom tile, clip ridge ash, gray back, watch board, etc.	It can buffer the external temperature, heat insulation, heat preservation, windproof, rainproof, and so on.

Table 2. Building envelope-size table

Name	L/mm	W/mm	H/mm
Building body	5366	5554	6816
Window 1 (west side)	1982	2088	---
Window 2 (south side)	3812	2261	---
Floor tiles/pc	550	400	53
	517	510	53

Note: The thickness of the east-west wall is 505 mm; the thickness of the north-south wall is 624 mm

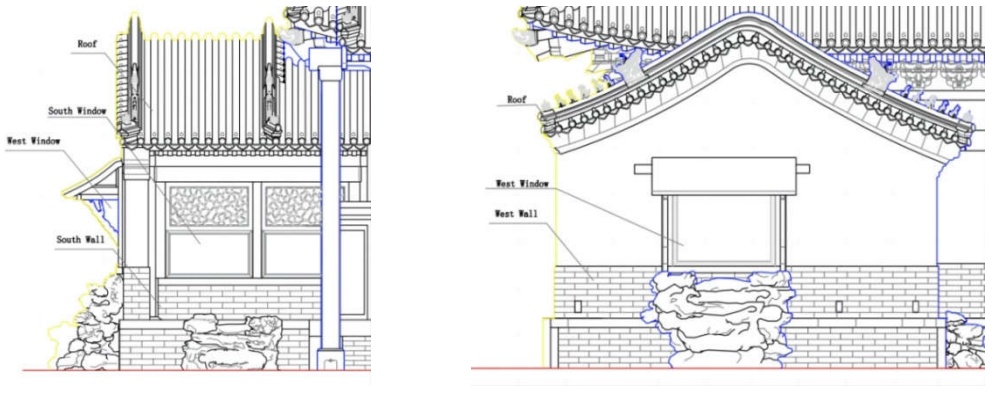

(**a**) (**b**)

Figure 2. Elevation of a palace-style wooden ancient building in Beijing: **(a)**South elevation **and (b)** West elevation.

Preprints (www.preprints.org) | NOT PEER-REVIEWED | Posted: 18 May 2023 doi:10.20944/preprints202305.1338.v1

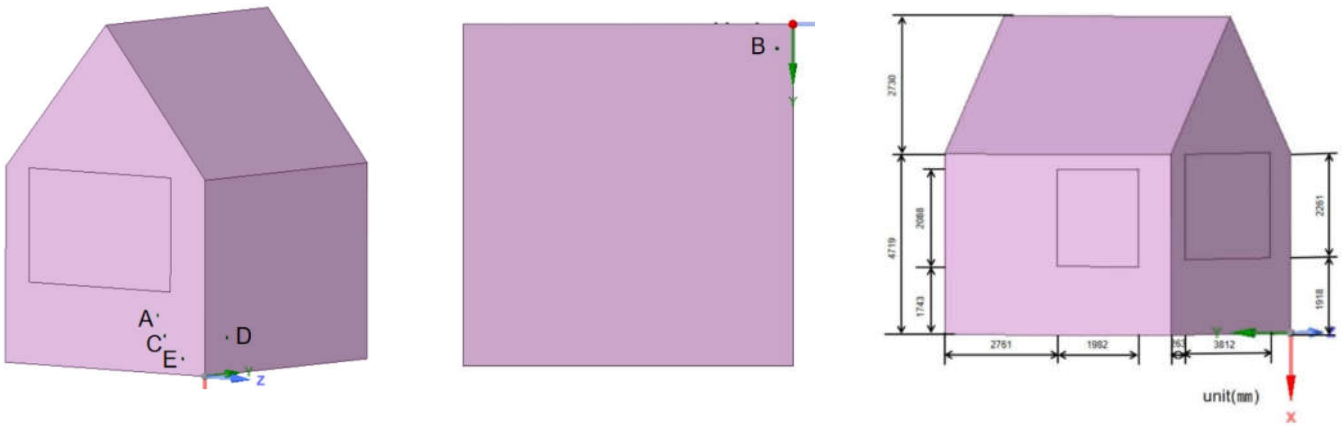

(a) (b) (c)

Figure 3. Structure of a palace-style wooden ancient building in Beijing: **(a)** South corner sample point , **(b)** Ground sample point and **(c)** Architectural model dimensional drawing.

3.2. Mathematical model

3.2.1. Basic assumptions

In this study, the ground and wall are set as the wet source, and the effects of ground soil moisture and wall humidity on the relative humidity inside the room are simulated respectively. To simplify the simulation, the actual physical process is assumed as follows.

(1)The underground river and the wall are wet sources.

(2) The floor and the wall are the water vapor flow inlet and the two windows are the gas outlets.

(3) The building interior is natural convection, and the indoor airflow is low-speed flow, which is regarded as an incompressible fluid [26] and satisfies the ideal gas equation of state.

(4) The water vapor mass fraction of the windows is set as the outdoor water vapor mass fraction.

3.2.2. Governing equations

Based on the physical model and basic assumptions, the governing equations in this paper are as follows.

Continuity equation:

$$div\ (\boldsymbol{U})\ =0 \tag{2}$$

$$div(u\boldsymbol{U}) = -\frac{1}{\rho}\frac{\partial p}{\partial x} + div(\nu \boldsymbol{grad} u) \tag{3}$$

Momentum equation:

$$div(v\boldsymbol{U}) = -\frac{1}{\rho}\frac{\partial p}{\partial y} + div(\nu \boldsymbol{grad} v) \tag{4}$$

$$div(\omega\boldsymbol{U}) = -\frac{1}{\rho}\frac{\partial p}{\partial z} + div(\nu \boldsymbol{grad} \omega) \tag{5}$$

Energy equation:

Preprints (www.preprints.org) | NOT PEER-REVIEWED | Posted: 18 May 2023 doi:10.20944/preprints202305.1338.v1

$$div(\rho T\boldsymbol{U}) = div\left(\frac{\lambda}{c_p}\boldsymbol{grad}T\right) + S_T \tag{6}$$

The ideal gas equation of state:

$$p = \rho RT \tag{7}$$

Where: is the fluid density, g/cm³. c_p is the specific heat capacity of fluid, $J/(kg \cdot K)$, λ is the thermal conductivity, $W/(m \cdot K)$ and $\boldsymbol{U}$ is the velocity vector. T is the thermodynamic temperature, K. ν is the kinematic viscosity of the fluid, m^2/s and S_T is the viscous dissipation term.

Due to the existence of the moat, the ground dissipates moisture. The windows of ancient buildings are made of wooden materials, which have poor sealing performance, resulting in a pressure difference between indoors and outdoors, causing some moisture to dissipate and diffuse from the outside to the inside. Therefore, in the simulation procedure, it is considered that the airflow in the ancient building blows upward from the ground. The standard model is used for simulation analysis [27]. In the near wall region, the flow state is laminar and has a low Reynolds number, with a ground average Reynolds number of 1.2109, which the wall function method is used for processing.

The floor and walls are made of grey bricks. The thermal conductivity of grey brick is $0.265W/(m \cdot K)$. The steam diffusion coefficient is $2.92 \times 10^{13} kW \cdot kg/(Pa \cdot m \cdot s)$. The heat flux density of the enclosure structure and the parameters of the indoor environment are shown in Tables 3 and 4.

Table 3. Heat flux density values of the enclosure structure

Designation		Heat flux q（W/m²）
Ground		1.50
Wall	North-South Wall	0.68
	East-West Wall	0.84
	Average	0.76

Table 4. Indoor environmental parameters table

Environment		Temperature/℃	Relative humidity/ %	Humidity content / g/kg dry air	The partial pressure of water vapor /kPa	Mass fraction of water vapor /%
Indoor	Center	24.7	75	14.67	2.3347	0.0145
	Ground	23.3	81.5	15.97	2.5371	0.0157
	Interior wall	24.7	92	18.09	2.8639	0.0167

3.3. Grid Partitioning and Irrelevance Verification

3.3.1. Grid division

Grid generation is very important in CFD (Computational Fluid Dynamics) simulation, which seriously affects the accuracy of CFD simulation by the quality of the generated grid [17]. In this work, a combination of tetrahedral and hexahedral grid types is used to mesh the building. The length (X) of the computational region is 6.816 m, the width (Y) is 5.554 m, and the height (Z) is 5.366 m. The number of grids in the X-direction is 97, the number of grids in the Y-direction is 79, and the

Preprints (www.preprints.org) | NOT PEER-REVIEWED | Posted: 18 May 2023 doi:10.20944/preprints202305.1338.v1

number of grids in the Z-direction is 77. The average value of this grid quality is 0.77, the grid cell size is 0.07 m, and the number of grids is 1,085,324. At the same time, adding boundary conditions and local encryption were used. The grids of the ground and the south corner of the palace-style building were encrypted, and the number of grids after encryption is 3,307,497. The results of local encryption are shown in Figure 4(a). The results of grid division are shown in Figure 4(b).

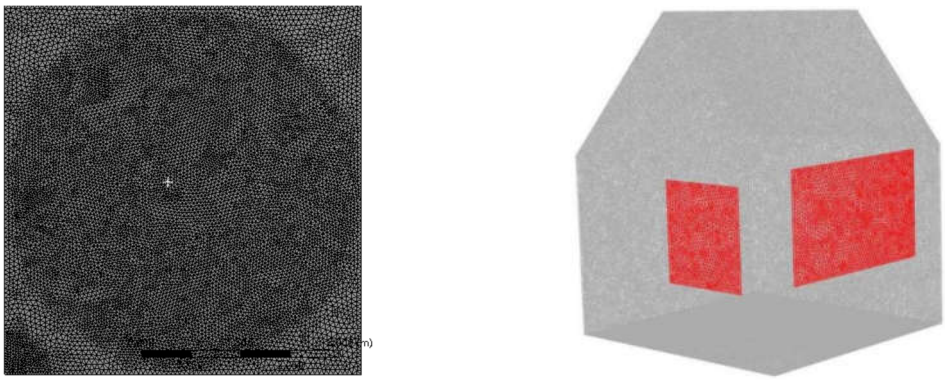

(**a**) (**b**)

Figure 4. Grid division of a palace-style ancient building model in Beijing: **(a)** Local encrypted grid division and **(b)** Overall meshing diagram.

3.3.2. Grid independence verification

To ensure the accuracy of the calculation results, the generated grids are verified for independence [26]. The following grids all converge monotonically, which are presented in Table 5. Comparing the data in Table 5, the grid independence verification is performed with the value of the average relative humidity on the ground as the reference variable. Grade 3 is closer to grade 1 than the other grades in terms of average relative humidity. In addition, the calculation time of grade 3 is much less than that of grade 1, which can reduce the calculation time to a certain extent. Therefore, grade 3 is selected for the simulation study in this work. At this time, the number of grids is about 1.08 million, the grid cell size is 0.07 m and the grid quality is good, which can meet the requirements of calculation accuracy.

Table 5. Data statistics of mesh verification

Grid classification levels	Grid size/m	Number of meshes/piece	Ground average temperature/℃	Ground average relative humidity/%
1	0.05	17315932	23.3	79.69638
2	0.06	1594340	23.3	79.63364
3	0.07	1085324	23.3	79.66715
4	0.08	779490	23.3	79.60327
5	0.09	583620	23.3	79.59776

3.4. Initial working conditions

The outdoor relative humidity range is 45.45 % to 87.89 %.

The range of relative humidity is simulated by changing the water vapor mass fraction, with a gradient of 0.02 %. The effects of ground soil relative humidity, outdoor ambient temperature, and wall relative humidity on indoor relative humidity are investigated. The boundary conditions are set as follows.

(1) West window and South window are set as the pressure outlets. The outdoor humidity is 67.17 %, and the water vapor mass fraction is 0.0142 %.

Preprints (www.preprints.org) | NOT PEER-REVIEWED | Posted: 18 May 2023 doi:10.20944/preprints202305.1338.v1

(2) Ground and wall are set as the mass flow inlet, and the mass flow rate is 0.3 m/s.

(3) The wall temperature is set to 26.3 °C and the ground temperature is 23.3 ℃. The water vapor mass fraction of ground and wall are 0.0145 % and 0.0167 %.

4. Results and Discussion

4.1. Mathematical model accuracy verification

Due to management limitations, testing of indoor temperature and humidity in the ancient building cannot be implemented. Wall mold refers to a fungal community that parasitizes on the surface of walls in the form of a microbial community and propagates in large quantities, using the available carbon and nitrogen sources in the wall skin layer (usually referred to as putty layer and topcoat layer) at appropriate temperatures (25 ℃ to 30 ℃) [28-31] and humidity (65 % to 95 %) [32], usually presenting black, green, red, and yellow fur forms. Wall mold can cause uneven walls, skin corrosion, peeling and foaming of decorative layers, as well as softening and powdering of building materials, resulting in reduced performance of insulation materials. It is seen that the presence of wall mold not only affects the aesthetics of buildings, but also damages the building structure and even poses a serious threat to the service life of the building. In this work, the simulated results of temperature and humidity at the growth point of wall mold are compared with the empirical values of temperature and humidity that are suitable for wall mold growth, and then determine the accuracy of the model.

Thus, five local points A (-0.5,0, -0.5), B (0,0.1, -0.15), C (-0.4,0, -0.3), D (-0.3,0.3, 0), E (-0.2,0, -0.15) are selected for the growth of wall mold on the indoor south wall corner and adjoining floor of ancient buildings, according to the results of the on-site investigation in Figure 5(a). The simulation results of local temperature and humidity are shown in Figure 5.

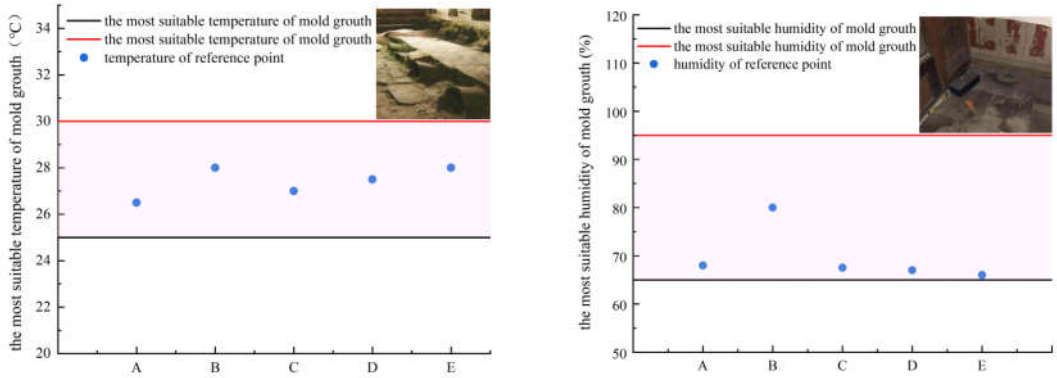

Figure 5. Analysis graph of localized points: **(a)** Temperature and **(b)** Relative humidity.

In Figure 5(a), the blue dots indicate the temperature values of the five points in the south wall corner, the black line represents the lowest temperature suitable for mold growth, the red line represents the highest temperature suitable for mold growth, and the pink area between the black line and the red line shows the temperature zone suitable for mold growth. All five points are within this temperature zone. In Figure 5(b), the blue dots indicate the relative humidity values of the five points in the south wall corner, the black line represents the lowest relative humidity suitable for mold growth, the red line represents the highest relative humidity suitable for mold growth, and the area in pink between the black line and the red line represents the relative humidity zone suitable for mold growth. All five points are within this relative humidity zone. Therefore, as can be seen from Figure 5, it is determined that the specific location of mold growth in ancient buildings is on the ground and in each corner of the walls. The simulation results of temperature and humidity at the selected locations for wall mold growth are consistent with empirical values.

Besides, according to the relevant data from actual measurements, the indoor relative humidity of the ancient building is close to 100 % in July and August in summer. At this point, the accuracy of

Preprints (www.preprints.org) | NOT PEER-REVIEWED | Posted: 18 May 2023 doi:10.20944/preprints202305.1338.v1

the model can also be verified by using the actual measured data of indoor relative humidity, and the average relative humidity of each cross-section is obtained by simulation as follows.

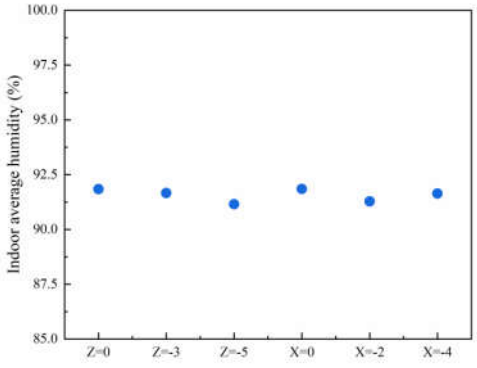

Figure 6. Average indoor relative humidity for each section.

As can be seen from Figure 6 above, the average indoor relative humidity for each section range from 91.1 % to 92.5 %, which are all greater than 90 % and close to 100 %. The results show that the data derived from the simulations are consistent with the measured data with small deviations. The accuracy of the simulation results was verified based on the measured data.

4.2 The indoor temperature and humidity distribution in initial working conditions

In this work, under the initial working conditions of ancient buildings (outdoor temperature of 26.3 ℃, outdoor relative humidity of 67.17 %), the indoor temperature and humidity distribution of ancient buildings are simulated.

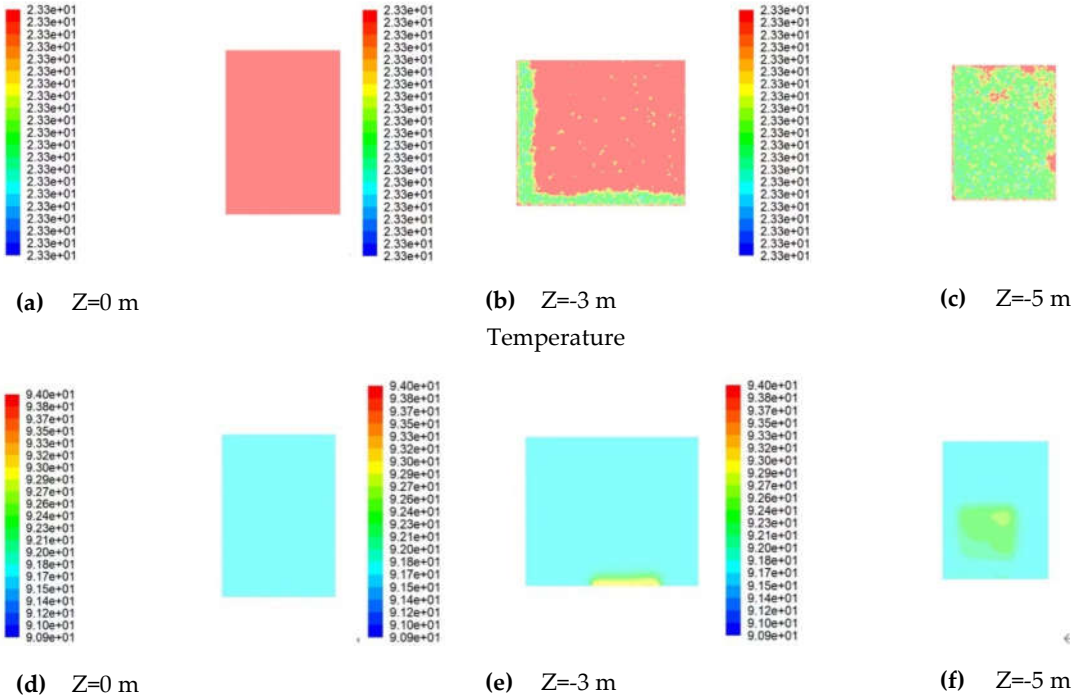

(a) Z=0 m **(b)** Z=-3 m **(c)** Z=-5 m

Temperature

(d) Z=0 m **(e)** Z=-3 m **(f)** Z=-5 m

Relative humidity

Figure 7. Indoor temperature and relative humidity distribution in the vertical direction

The distribution of temperature and relative humidity at Z=0 m, Z=-3 m, and Z=-5 m in the vertical direction are shown in Figure 7respectively. The temperature and relative humidity distribution inside the wall are not uniform at Z=0 m (east wall), the temperature around the east wall is 23.3 ℃ and the relative humidity is up to 91.8 % as can be seen in Figure 7(a)(d), the relative

Preprints (www.preprints.org) | NOT PEER-REVIEWED | Posted: 18 May 2023 doi:10.20944/preprints202305.1338.v1

humidity in the middle part of the room is unchanged, which mainly because its moisture content is evenly distributed. Figure 7(b) shows that the temperature is unchanged. And Figure 7(e) shows the relative humidity of the south and the west windows is higher than that at the same vertical plane which is due to that the windows are wooden, there are gaps to cause penetration so that the moisture content of the windows is high.

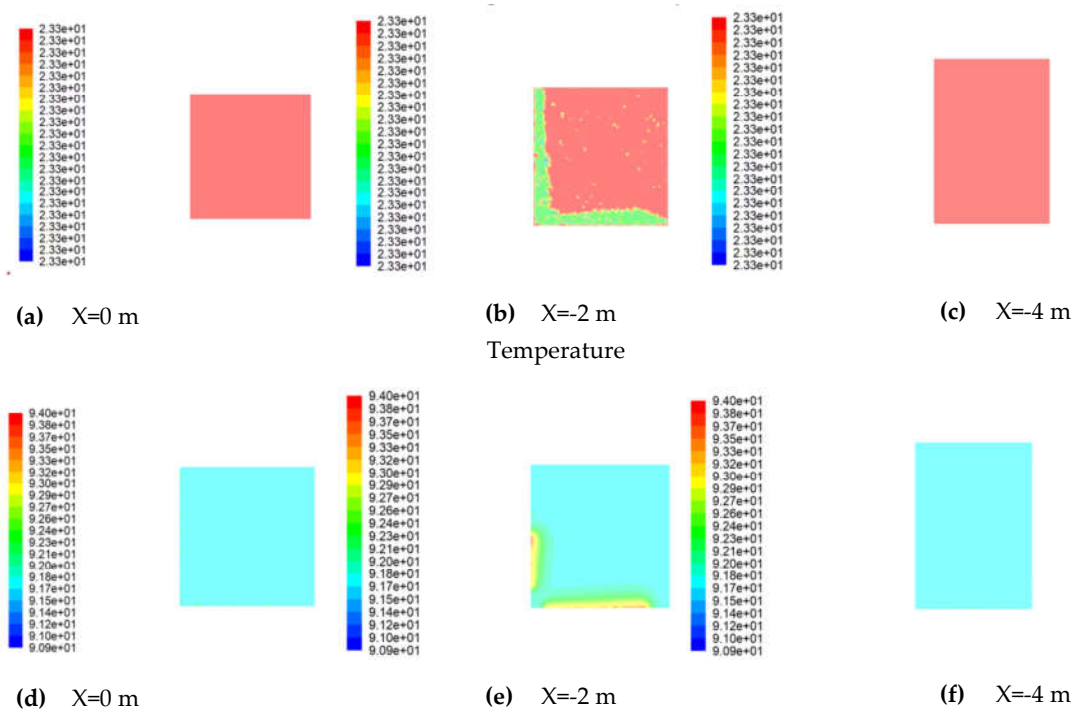

Figure 8. Indoor temperature and humidity distribution in the horizontal direction.

The distribution of temperature and relative humidity in the horizontal direction at X=0 m, X=-2 m, and X=-4 m is shown in Figure 8 respectively. Analysis of Figures 8(a), (b), and (c) above show that the room temperature maintains at 23.3 ℃ and remains the same. From Figure 8(d), it can be seen that the relative humidity of the ground remains unchanged at 91.7 %. This is mainly due to the presence of a moat on the ground, which makes its moisture content evenly distributed. From Figure 8(e), it can be seen that the relative humidity values at the south and west windows are larger than those at the rest of the plane, which is due to the infiltration effect of the windows that makes their humidity greater. From Figure 8(f), it can be seen that the relative humidity on the roof remains constant and the indoor relative humidity value is higher.

The comprehensive analysis reveals that the indoor average temperature is 23.3 ℃, and the indoor relative humidity range is between 91.7 % and 93.5 %. Overall, the temperature fluctuation in the interior of the ancient building is small, while the relative humidity fluctuates widely. Therefore, the following section focuses on the effect of each factor on indoor humidity. And controlled variable method is taken to investigate changes in humidity.

4.3 Effect of outdoor humidity on indoor heat and moisture transfer

The humidity of the soil and wall is set as the initial state. With the difference in outdoor humidity, the indoor humidity is shown in Figure 9 (a)(b). Due to the ancient age of this historic building, outdoor air enters the interior through windows, which are made of paper material and have a significant degree of damage. Thus, the outdoor humidity environment is an important influencing factor on the indoor humidity of the ancient building.

Preprints (www.preprints.org) | NOT PEER-REVIEWED | Posted: 18 May 2023 doi:10.20944/preprints202305.1338.v1

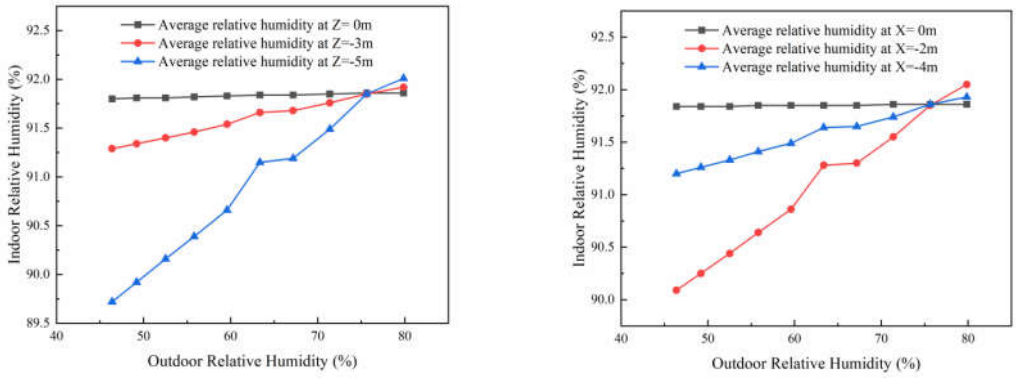

(**a**) (**b**)

Figure 9. Effect of outdoor humidity on the humidity in the horizontal and vertical direction of the room.

As can be seen from Figure 9(a), when the outdoor humidity is certain, the indoor relative humidity is observed to change in the vertical direction from east to west (Z=0 m to Z=-5 m). When the outdoor humidity is less than 75.6 %, the average indoor relative humidity shows a trend of gradual decrease. And when the outdoor humidity is greater than 75.6 %, the average indoor relative humidity shows a gradually increasing trend. When located in the same vertical plane, with the increase of outdoor humidity, the average indoor relative humidity increases significantly at Z=-5 m. At Z=-3 m, the trend of the average indoor relative humidity increases more slowly than that at Z=-5 m. At Z=0 m, the average indoor relative humidity remains unchanged.

As can be seen from Figure 9(b), when the outdoor humidity is certain, the change of indoor relative humidity in the horizontal direction from the ground to the roof (X=0 m to X=-4 m) is observed. When the outdoor humidity is less than 75.6 %, the average indoor relative humidity shows a trend of first decreasing and then gradually increasing, and the change of decreasing is larger. At outdoor humidity greater than 75.6 %, the average indoor relative humidity showed a trend of first increasing and then gradually decreasing. Therefore, it was concluded that the average relative humidity at ground level was the highest. When located in the same horizontal plane, with the increase of outdoor humidity, the average indoor relative humidity is the highest and remains the same at X=0 m. At X=-2 m, the average indoor relative humidity increases significantly. At X=-4 m, the average indoor relative humidity shows a slowly increasing trend.

4.4 Effect of soil moisture on heat and moisture transfer

Xu et al. [33] carried out experiments on the effect of coupled heat and moisture transfer on soil heat storage systems and confirmed that ignoring the moisture migration and temperature dependence of soil thermal conductivity would lead to a low predicted value of the numerical model, and the influence of initial soil moisture on coupled heat and moisture transfer should be considered. In this paper, the influence of soil moisture on the humidity in different directions in the room was simulated by changing the mass fraction of groundwater vapor (soil moisture).

Preprints (www.preprints.org) | NOT PEER-REVIEWED | Posted: 18 May 2023 doi:10.20944/preprints202305.1338.v1

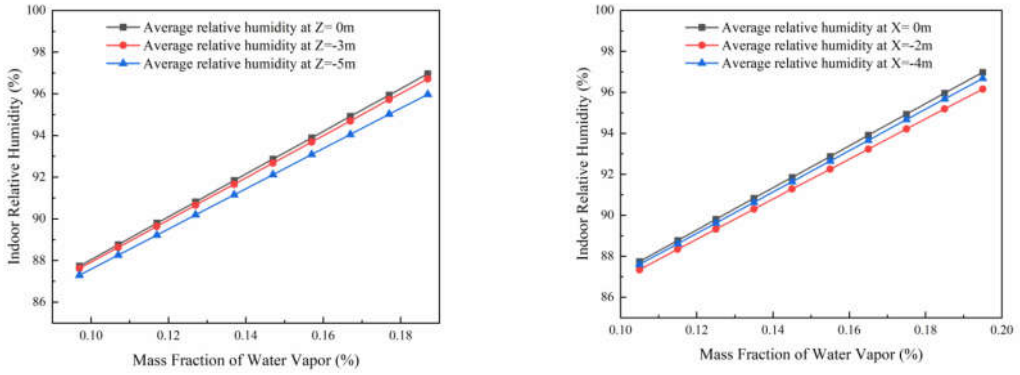

(**a**) (**b**)

Figure 10. Effect of soil moisture on the humidity in the horizontal and vertical direction of the room.

As can be seen from Figure 10(a), when the soil humidity is certain, the change of indoor relative humidity in the vertical direction from east to west (Z = 0 m to Z = -5 m) is observed. The average indoor relative humidity gradually decreases, but the decrease is small. When located in the same vertical plane, the average indoor relative humidity gradually increased with the increase of soil moisture, and the trend of increase was almost the same in each plane.

As can be seen from Figure 10(b), when the soil humidity is certain, the average indoor temperature shows a trend of first decreasing and then increasing when observing the change of indoor temperature and humidity in the horizontal direction from the ground to the roof (X=0 m to X=-4 m), but the change is smaller. When located in the same horizontal plane, the average indoor relative humidity increases gradually with the increase of soil humidity.

4.5 Effect of wall humidity on indoor heat and humidity transfer

With time, the porosity of the ancient building envelope will become larger, and its moisture storage capacity will also be enhanced. In addition, excessive humidity in the building envelope can lead to damage to building materials and mold growth [34]. It is also a factor that produces wall mold, as it migrates to the indoor environment. Therefore, the influence of wall humidity on the humidity in different directions of the room was simulated by changing the water vapor mass fraction (changing the wall humidity) of the wall.

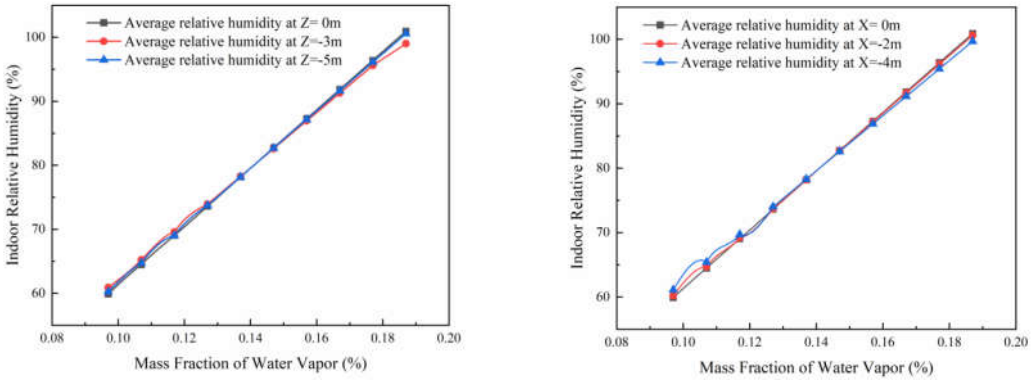

(**a**) (**b**)

Figure 11. Effect of wall humidity on the average humidity in the horizontal and vertical direction of the room.

As can be seen from Figure 11(a), the indoor relative humidity values on different planes are the same, so the relative humidity of the whole room can be analyzed by the above figure. From Figure 11 (a)(b), it can be seen that as the humidity of the walls increases, the relative humidity in the room also increases gradually. This is due to the moisture transfer from the walls, which makes the humidity in the room also increase gradually.

Preprints (www.preprints.org) | NOT PEER-REVIEWED | Posted: 18 May 2023 doi:10.20944/preprints202305.1338.v1

From the analysis of indoor relative humidity law in 4.4 and 4.5, it can be seen that when the ground or wall water vapor mass fraction decreases (ground soil or wall humidity decreases), the average indoor relative humidity decreases, when the conditions of building protection and maintaining the original appearance of the building can be met. Therefore, the relative humidity of the indoor environment can be reduced by lowering the ground soil moisture or wall humidity.

4.6 The sensitivity of factors

While the effect patterns of outdoor environmental humidity, soil moisture, and wall humidity on indoor relative humidity have been obtained through simulation, the sensitivity of each factor requires correlation analysis takes statistical methods [35], with indoor relative humidity as the target (significant test level of 0.01). Outdoor ambient humidity, soil moisture, and wall humidity are set as the reference series X_0, and indoor ambient relative humidity is set as the comparison series $X_i(k)$, respectively. Based on the existing correlation empirical equations [36,37], the calculation steps of the correlation analysis are as follows.

Relation coefficient:

$$\gamma_i(k) = \frac{\min_i \min_k \Delta_i(k) + \xi \max_i \max_k \Delta_i(k)}{\Delta_i(k) + \xi \max_i \max_k \Delta_i(k)} \quad (8)$$

Where: $\Delta_i(k) = |X_0'(k) - X_i'(k)|$, $\xi \in (0,1)$ is the resolution factor, which usually takes the value of 0.5.

Correlation degree:

$$R_i = \frac{1}{n}\sum_{k=1}^{n} \gamma_i(k), i = 1,2,3,...,m; k = 1,2,3,...,n \quad (9)$$

Table 6. Correlation analysis result

Dependent variable	Indoor relative humidity
Correlation coefficient with outdoor environmental humidity	0.486
Correlation coefficient with soil moisture	0.995
Correlation coefficient with wall humidity	0.993

From Table 6, it can be seen that the correlation of outdoor ambient humidity to indoor relative humidity is weak; while the correlation of soil humidity and wall humidity to indoor relative humidity is strong, and the correlation of wall and indoor relative humidity is lower than that of soil by 0.002. This paper mainly focuses on the problem of wet building floors and high indoor relative humidity. Therefore, it can be concluded that soil moisture and wall moisture are the main factors affecting indoor relative humidity.

4.7 Indoor temperature and humidity distribution after moisture-proof treatment

According to related studies [38394040], antimicrobial and hydrophobic coatings can be used to reduce room humidity by coating and protecting the moldy areas of bricks without affecting the appearance of ancient buildings. For example, SiO_2-TiO_2 hybrid fluorinated B-72, lime putty mortar (ASPL and ASPL/PP series), etc. This coating has better resistance to acid, alkali, salt, and UV light as well as inhibition of mold growth. Ground and walls as an example of wet source, obtained from Figure 16, when the water vapor mass fraction of 0.0105 % (ground soil relative humidity of 59.02 %)

Preprints (www.preprints.org) | NOT PEER-REVIEWED | Posted: 18 May 2023 doi:10.20944/preprints202305.1338.v1

when the wall water vapor mass fraction of 0.0107 % (wall relative humidity of 60 %), the relative humidity of the ancient building interior is located in 60.2 % to 78.8 %, in line with the requirements of indoor relative humidity under summer working conditions. Indoor ground temperature and humidity distribution, as shown in Figure 12, the temperature at the ground is 23.3 ℃, with an average relative humidity of 60.32 %. As can be seen in Figure 12(a), after the damp-proofing treatment, the relative humidity of the ancient building interior was reduced from 90.9 % to 94.0 % to 60.2 % to 78.8 %, and the relative humidity decreased and met the requirements of indoor relative humidity under summer working conditions.

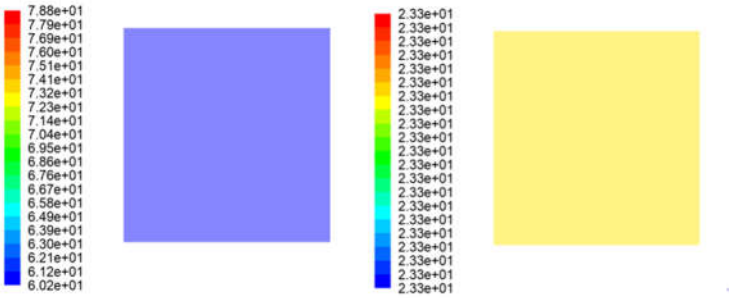

Figure 12. Indoor ground temperature and humidity distribution picture: **(a)** Humidity and **(b)** Temperature.

5 Conclusion

To solve the problem of mold growth causing damage to the architectural style of an ancient palace in Beijing, a simulation study of the indoor heat and humidity transfer characteristics of ancient buildings was carried out by using the ANSYS numerical simulation research method. The results of the influence parameters of the indoor humidity and the proposed protective measures were obtained as follows.

(1) Indoor relative humidity varies with the trend of outdoor humidity; it increases with the increase of soil humidity; it increases with the increase of wall humidity.

(2) Soil moisture and wall moisture are the main factors affecting the change in indoor relative humidity.

Protective measures:

(1) Placing moisture-absorbing materials with reduced surface relative humidity in the humid indoor part of the building to improve the ground moisture level and reduce ground condensation;

(2) Blocking the floor openings to reduce the degree of ground moisture aggravated by capillary action;

(3) Applying antibacterial and hydrophobic coatings to walls and floors.

Author Contributions: All authors contributed to this paper. Conceptualization, F.L. and X.Z.; methodology, writing—original draft preparation, resources, supervision, F.L.; software, J.Z.; validation, X.Z., J.Z.; formal analysis, Y.L.; writing—original draft preparation, supervision, F.L.; writing—review and editing, G.W.; All authors have read and agreed to the published version of the manuscript.

Funding: This research received no external funding.

Data Availability Statement: No new data were created or analyzed in this study.

Acknowledgments: We also would like to thank the anonymous reviewers for their valuable comments and suggestions that lead to a substantially improved manuscript.

Conflicts of Interest: The authors declare no conflict of interest.

References

1. Wei, K.; Yang, W.Y.; Zhou, B.; Wang, K.; Sun, J.Z.; Sun, X.K.; Xu, M.; Chen, Q.Q.; Qiu, B.; Wang, W.; Wang, X. The color change analysis of historic wooden remains after fire-suppression by fluorinated chemical gases. Herit. Sci. 2021, 9:93. https://doi.org/10.1186/s40494-021-00565-6.
2. Qiu, Y.H. 3D Reconstruction and Intelligent Digital Conservation of Ancient Buildings Based on Laser Point Cloud Data. J. Electr. Comput. Eng. 2022, 2022, 7182018. https://doi.org/10.1155/2022/7182018.
3. Rubeis, T.D.; Nardi, I.; Muttilloa, M.; Paoletti, D. The restoration of severely damaged churche-Implications and opportunities on cultural heritage conservation, thermal comfort and energy efficiency. J. Cult. Herit. 2020, 43,186-203.https://doi.org/10.1016/j.culher.2019.11.008.
4. Santosuosso, P. A satisfaction-based model for risk indexing in cultural heritage conservation. J. Cult. Herit. 2022, 57, 173-183. https://doi.org/10.1016/j.culher.2022.08.007.
5. Fico, D.; Rizzo, D.; Casciaro, R.; Corcione, C.E. Historically Accurate Reconstruction of the Materials and Conservation Technologies Used on the Facades of the Artistic Buildings in Lecce (Apulia, Italy). Materials. 2022,15, 3658. https://doi.org/10.3390/ma15103658.
6. Wang, X.Y.; Wang, J.; Wang, J.H.; Sheng, G.H. Experimental and Numerical Simulation Analyses of Flame Spread Behaviour over Wood Treated with Flame Retardant in Ancient Buildings of Fuling Mausoleum, China. Fire. Technol. 2022. https://doi.org/10.1007/s10694-022-01311-5.
7. Huai, C.P.; Xie, J.C.; Liu, F.; Du, J.T.; Chow, D.H.C.; Liu, J.P. Experimental and Numerical Analysis of Fire Risk in Historic Chinese Temples: A Case in Beijing. Int. J. Archit. Herit. 2022, 16, 1844-1858. https://doi.org/10.1080/15583058.2021.1916648.
8. Talbot, R.; Picco, M.; Greenfield, D.; Ashton, P.; Arbuthnot, E.; Hashemi, A. Historic Churches and Their Hygrothermal Environment: A Review of Criteria Related to Building Fabric, Artefacts, Artwork and Occupants. Sustainability. 2022, 14, 7822. https://doi.org/10.3390/su14137822.
9. Steeman, H.J.; Belleghem, M.V.; Janssens, A.; Paepe, M.D. Coupled simulation of heat and moisture transport in air and porous materials for the assessment of moisture related damage. Build. Environ. 2009, 44, 2176-2184. https://doi.org/10.1016/j.buildenv.2009.03.016.
10. Belleghem, M.V.; Steeman, M.; Willockx, A.; Janssens, A.; Paepe, M.D. Benchmark experiments for moisture transfer modelling in air and porous materials. Build. Environ. 2011, 46, 884–898. https://doi.org/10.1016/j.buildenv.2010.10.018.
11. Huang, H.; Kato, S.; Hu, R.; Ishida, Y. Development of new indices to assess the contribution of moisture sources to indoor humidity and application to optimizati-on design: Proposal of CRI(H) and a transient simulation for the prediction of i-ndoor humidity, Build. Environ. 2011, 46, 1817-1826. https://doi.org/10.1016/j.buildenv.2011.03.002.
12. Liu, W.Q. The Evolution of Cold Adaptation Technology within Ancient Buildings in Amur River Basin Viewed from Archaeology. Int. J. Environ. Res. Public Health. 2022, 19, 14470. https://doi.org/10.3390/ijerph192114470.
13. Teodosiu, C.; Hohota, R.; Rusaouën, G.; Woloszyn, M. Numerical prediction of ind-oor air humidity and its effect on indoor environment. Build. Environ. 2003, 38, 655-664. https://doi.org/10.1016/S0360-1323(02)00211-1.
14. Bi, W.B.; Yan, Z.F.; Zhang, Z.M.; Yao, S.S.; Zhang, J.J.; Wang, X.D. Modeling and numerical simulation of heat and mass transfer in the cave wall of the Mogao -Grottoes in China. Build. Environ. 2021, 201, 108003. https://doi.org/10.1016/j.buildenv.2021.108003.
15. Balocco, C.; Grazzini, G. Numerical simulation of ancient natural ventilation syste-ms of historical buildings. A case study in Palermo. J. Cult. Herit. 2009, 10, 313-318. https://doi.org/10.1016/j.culher.2008.03.008.
16. Li, S.; Xie, H.R.; Ma, Y.; Hokoi, S.C.; Li, Y.H. Assessing the deterioration risk of polychrome clay sculptures based on the hygrothermal environment: A case study of Baosheng temple, China. Case Stud. Constr. Mater. 2022, 17, e01287. https://doi.org/10.1016/j.cscm.2022.e01287.
17. Cao, L.N.Y.; Cao, J.J.; Lee, S.C.; Zhang, Y.W.; Tie, X.X. Numerical Simulation of the Micro Environment in the Han Yang Mausoleum Museum. Aerosol. Air. Qual. Res. 2012, 12, 544-552. https://doi.org/10.4209/aaqr.2011.12.0240.
18. Huijbregts, Z.; Schellen, H.; Schijndel, J.V.; Ankersmit, B. Modelling of heat and moisture induced strain to assess the impact of present and historical indoor climate conditions on mechanical degradation of a wooden cabinet. J. Cult. Herit. 2015, 16, 419-427. https://doi.org/10.1016/j.culher.2014.11.001.
19. Napp, M.; KalameesA, T. Energy use and indoor climate of conservation heating, dehumidification and adaptive ventilation for the climate control of a mediaeval c-hurch in a cold climate. Energy. Build. 2015, 108, 61–71. https://doi.org/10.1016/j.enbuild.2015.08.013.
20. Wei, L.; Ma, Y.; Guo, Z.M.; Ding, J.J.; Jin, G.W.; Gu, A.; Lei, Y. Application of Advanced Analytical Techniques in Organic Cultural Heritage: A Case Study of Ancient Architecture Relics in the Palace Museum (Beijing). Coatings. 2022, 12, 636. https://doi.org/10.3390/coatings12050636.

21. Zhang, X.G.; Zhang, S.; Chen, H.Y. Research and Analysis of the Building Environment in the Conservation of Yang Xin Hall Area in the Palace Museum. Traditional Chinese Architecture and Gardens (Protection of Cultural Heritage). 2018, 02, 31-36. (in Chinese).
22. Xu, Y.S.; Zeng, Z.T.; Sun, D.A. Experimental and numerical investigation on the effect of heat and moisture coupling migration of unsaturated lateritic clay for the soil thermal storage system. Energy. Build. 2022, 276, 112499. https://doi.org/10.1016/j.enbuild.2022.112499.
23. Zhao, P.; Zhang, X.Z.; Qin, L.; Zhang, Y.S.; Zhou, L.Z. Conservation of disappearing traditional manufacturing process for Chinese grey brick: Field survey and laboratory study. Constr. Build Mater. 2019, 212, 531-540. https://doi.org/10.1016/j.conbuildmat.2019.03.317.
24. Chen, X.Y.; Ye, J.C.; Lu, G.H.; Qin, F.X. Study on field capacity distribution about soil of China. Water Resources and Hydropower Engineering. 2004, 35, 113-116+119. (in Chinese). https://doi.org/10.13928/j.cnki.wrahe.2004.09.033.
25. Specifications for soil moisture monitoring. Ministry of Water Resources of the P-eople's Republic of China. SL 364-2015. (in Chinese).
26. Xiong, J.; Li, A.G.; Liu, C.P.; Dong, J.G.; Yang, B.; Cao, J.J.; Ren, T. Probing the historic thermal and humid environment in a 2000-year-old ancient underground tomb and enlightenment for cultural heritage protection and preventive conservation. Energy. Build. 2021, 251, 111388. https://doi.org/10.1016/j.enbuild.2021.111388.
27. Vereecken, E.; Roels, S. Review of mould prediction models and their influence on mould risk evaluation. Build. Environ. 2011, 51, 296-310. https://doi.org/10.1016/j.buildenv.2011.11.003.
28. Zhang, G.Q.; Gu, A.; Wei, L. Regularity in distribution, and control, of pests in the hall of mental cultivation, the Forbidden City, Beijing, China. Herit. Sci. 2021, 2021, 111. https://doi.org/10.1186/s40494-021-00588-z.
29. Dallongeville, A.; Cann, P.L.; Zmirou-Navier, D.; Chevrier, C.; Costet, N.; Annesi-Maesano, I.; Blanchard, O.; Concentration and determinants of molds and allergens in indoor air and house dust of French dwellings. Sci. Total Environ. 2015, 536, 964-972. https://doi.org/10.1016/j.scitotenv.2015.06.039.
30. Menneer, T.; Mueller, M.; Sharpe, R.A.; Townley, S. Modelling mould growth in domestic environments using relative humidity and temperature. Build. Environ. 2022, 208, 108583. https://doi.org/10.1016/j.buildenv.2021.108583.
31. Li, Y.H. Huang, Z.; Petropoulos, E.; Ma, Y.; Shen, Y. Humidity governs the wall-inhabiting fungal community composition in a 1600-year tomb of Emperor Yang. Sci. Rep. 2020, 10, 8421. https://doi.org/10.1038/s41598-020-65478-z.
32. Ezeonu, I.M.; Noble, J.A.; Simmons, R.B.; Price, D.L.; Crow, S.A.; Ahearn, D.G. Effect of relative humidity on fungal colonization of fiberglass insulation. Appl. Environ. Microbiol. 1994. https://doi.org/10.1128/aem.60.6.2149-2151.1994.
33. Xu, Y.S. Zeng, Z.T.; Sun, D.A. Experimental and numerical investigation on the effect of heat and moisture coupling migration of unsaturated lateritic clay for the soil thermal storage system. Energy. Build. 2022, 276, 112499. https://doi.org/10.1016/j.enbuild.2022.112499.
34. Li, Y.H.; Kong, Z.Y.; Xie, H.R.; Ma, Y.; Mu, B.G.; Hokoi, S.C. Construction type influences features of rising damp of blue-brick masonry walls, Constr. Build. Mater. 2021, 284, 122791. https://doi.org/10.1016/j.conbuildmat.2021.122791.
35. Jacob, K.S. Statistical Methods in Psychiatric Research and SPSS, Indian J. Psychiatry. 2016, 58, 356. https://doi.org/10.4103/0019-5545.192008.
36. J. Ashraf, L.Q. Luo, M.K. Anser, Do BRI policy and institutional quality influence economic growth and environmental quality? An empirical analysis from South Asian- countries affiliated with the Belt and Road Initiative. Environ. Sci. Pollut. Res. 2022, 29, 8438-8451. https://doi.org/10.1007/s11356-021-16330-y.
37. Mausam, K.; Pare, A.; Ghosh, S.K.; Tiwari, A.K. Thermal performance analysis of hybrid-nanofluid based flat plate collector using Grey relational analysis (GRA): An approach for sustainable energy harvesting. Therm. Sci. Eng. Prog. 2023, 37, 101609. https://doi.org/10.1016/j.tsep.2022.101609.
38. Vacher, S.; Hernandez, C.; Bärtschi, C.; Poussereau, N. Impact of paint and wall-paper on mould growth on plasterboards and aluminum. Build. Environ. 2010, 45, 916-921. https://doi.org/10.1016/j.buildenv.2009.09.011.
39. Wang, K.Y.; Bu, N.J.; Zhen, Q.; Liu, J.B.; Bashir, S. Modified nano-SiO2/TiO2 hybrid fluorinated B-72 as antimicrobial and hydrophobic coatings for the conservation of ancient bricks. Constr. Build. Mater. 2023, 365, 130090. https://doi.org/10.1016/j.conbuildmat.2022.130090.
40. Branco, F.G.; Belgas, M.D.L.; Mendes, C.; Pereira, L.; Ortega, J.M. Characterization of Fresh and Durability Properties of Different Lime Mortars for Being Used as Masonry Coatings in the Restoration of Ancient Constructions. Sustainability. 2021, 13, 4909. https://doi.org/10.3390/su13094909.